

Lyman Continuum leakage from massive leaky starbursts: A different class of emitters?

NAMRATA ROY,¹ TIMOTHY HECKMAN,^{1,2} ALAINA HENRY,^{3,4} JOHN CHISHOLM,⁵ SOPHIA FLURY,⁶ CLAUS LEITHERER,³
MATTHEW J. HAYES,⁷ ANNE JASKOT,⁸ ZHIYUAN JI,⁹ DANIEL SCHAERER,^{10,11} BINGJIE WANG (王冰洁),^{12,13,14}
SANCHAYEETA BORTHAKUR,¹⁵ XINFENG XU,^{16,17} AND GÖRAN ÖSTLIN⁷

¹*Center for Astrophysical Sciences, William H. Miller III Department of Physics and Astronomy, Johns Hopkins University, Baltimore, MD, 21218*

²*School of Earth and Space Exploration, Arizona State University, Tempe, AZ, 85287*

³*Space Telescope Science Institute, 3700 San Martin Drive, Baltimore MD, 21218*

⁴*Center for Astrophysical Sciences, Department of Physics and Astronomy, Johns Hopkins University, Baltimore, MD, 21218*

⁵*Department of Astronomy, University of Texas at Austin, 2515 Speedway, Austin, Texas 78712, USA*

⁶*Institute for Astronomy, University of Edinburgh Royal Observatory, Blackford Hill, Edinburgh, EH9 3HJ, UK*

⁷*Department of Astronomy, Oskar Klein Centre, Stockholm University, AlbaNova University Center, 10691 Stockholm, Sweden*

⁸*Department of Astronomy, Williams College, Williamstown, MA 01267, USA*

⁹*Steward Observatory, University of Arizona, 933 N. Cherry Avenue, Tucson, AZ 85721, USA*

¹⁰*Observatoire de Genève, Université de Genève, Chemin Pegasi 51, 1290 Versoix, Switzerland*

¹¹*CNRS, IRAP, 14 Avenue E. Belin, 31400 Toulouse, France*

¹²*Department of Astronomy & Astrophysics, The Pennsylvania State University, University Park, PA 16802, USA*

¹³*Institute for Computational & Data Sciences, The Pennsylvania State University, University Park, PA 16802, USA*

¹⁴*Institute for Gravitation and the Cosmos, The Pennsylvania State University, University Park, PA 16802, USA*

¹⁵*School of Earth and Space Exploration, Arizona State University, 781 Terrace Mall, Tempe, AZ 85287, USA*

¹⁶*Department of Physics and Astronomy, Northwestern University, 2145 Sheridan Road, Evanston, IL, 60208, USA.*

¹⁷*Center for Interdisciplinary Exploration and Research in Astrophysics (CIERA), 1800 Sherman Avenue, Evanston, IL, 60201, USA.*

ABSTRACT

The origin of Lyman continuum (LyC) photons responsible for reionizing the universe remains a mystery, with the fraction of escaping LyC photons from galaxies at $z \sim 6$ to 12 being highly uncertain. While direct detection of LyC photons from this epoch is hindered by absorption from the intergalactic medium, lower-redshift analogs offer a promising avenue to study LyC leakage. We present Hubble Space Telescope Cosmic Origins Spectrograph (HST COS) observations of five low-redshift ($z \sim 0.3$) massive starburst galaxies, selected for their high stellar mass and weak [S II] nebular emission—an indirect tracer of LyC escape. Three of the five galaxies show LyC leakage, highlighting the reliability of weak [S II] as a tracer, especially in light of recent JWST discoveries of $z > 5$ galaxies with similarly weak [S II] emission. The dust-corrected LyC escape fractions ($f_{\text{esc,HI}}$), which represent the LyC photons that would escape in the absence of dust, range from 33% to 84%. However, the absolute escape fractions ($f_{\text{esc,tot}}$), which show the LyC photons escaping after passing through both neutral hydrogen HI absorption and dust attenuation, are significantly lower, ranging between 1% and 3%. This suggests that while the galaxies are nearly optically thin to HI, their high dust content significantly suppresses LyC photon escape. These [SII]-weak, massive leakers are distinct from typical low-redshift LyC emitters, showing higher metallicity, lower ionization states, more dust extinction and higher star formation surface densities. This suggests that these galaxies constitute a distinct population, likely governed by a different mechanism facilitating LyC photon escape. We propose that the feedback-driven winds in these compact starbursts create ionized channels through which LyC photons escape, aligning with a “picket-fence” model.

Keywords: Galaxies: emission lines – Galaxies: high-redshift – Galaxies: evolution

1. INTRODUCTION

The epoch of Reionization (EoR) is a critical phase in the history of the Universe when the intergalactic medium (IGM) changes its state from neutral to completely ionized

(see Robertson 2022, for a review). It also signifies the period when the first generation of massive stars and black holes form. Observations from cosmic microwave background (CMB), WMAP and Ly α forest absorption troughs in distant quasars bear evidence that the major part of the reionization occurred as early as $z \sim 12$, and lasted until $z \sim 6$ (e.g., Becker et al. 2001; Fan et al. 2006; Bañados et al. 2018; Mason & GLASS 2018; Planck Collaboration et al. 2020). But what are the primary sources for reionization? The early star forming galaxies are hypothesized to be the best candidates to supply the ionizing photons necessary for the Universe to be ionized (Bouwens et al. 2016). However, the fraction of these ionizing Lyman continuum (LyC) photons that are actually able to escape from dense neutral gas into the IGM is poorly constrained. An average LyC escape fraction (f_{esc}) of 20% or higher is required for star forming galaxies to be the major source for reionization (Bouwens et al. 2011; Robertson et al. 2015), although recent results show that the required f_{esc} do not need to be that high (Finkelstein et al. 2019; Atek et al. 2024). It is however crucial to find star forming galaxies with high LyC escape to confirm their role in reionization.

Although many attempts have been made to observationally constrain the escape fraction in star forming galaxies across a wide range of redshift, most of the early observations yielded upper limits only with a few detections, indicating $f_{\text{esc}} < 3\%$ (Leitherer et al. 1995; Deharveng et al. 2001; Malkan et al. 2003; Alavi et al. 2020). With a more extensive search program in recent years using the Hubble Space Telescope (HST) Cosmic Origins Spectrograph (COS; Green et al. 2012), convincing detections of LyC leaking emission have been found in a few tens of sources, mostly from local ($0.2 < z < 0.4$) starbursts, “Green Pea” galaxies, and Lyman break analogs (Heckman et al. 2005; Hoopes et al. 2007; Iwata et al. 2009; Borthakur et al. 2014; Izotov et al. 2016b,a, 2018a,b, 2021; Wang et al. 2019, 2021; Flury et al. 2022a; Xu et al. 2022). Notably, the recently completed Low Redshift Lyman Continuum Survey (LzLCS; Saldana-Lopez et al. 2022; Flury et al. 2022a,b) assembled a sample of 66 star forming LyC leaking “candidate” galaxies from the Sloan Digital sky survey (SDSS; York et al. 2000) and Galaxy Evolution Explorer (GALEX; Martin et al. 2005), which were observed with HST/COS. The program added 35 new LyC detections with 97.7% confidence. These Lyman continuum emitters (LCEs) serve as the largest Lyman Continuum Emitters sample detected to date.

As the confirmed direct detections of LyC escape have increased over the last couple of years, correlations have emerged between f_{esc} and their host galaxy properties. For example, there is a clear trend for leaky galaxies with high f_{esc} to preferentially have low stellar mass ($< 10^9 M_{\odot}$), high star formation rate (SFR), low metallicities ($< 1/3$

solar) strong nebular emission lines, highly ionized gas ($[\text{OIII}]5007/[\text{OII}]3727 > 3$), low-dust attenuation and strong Ly α emission (Overzier et al. 2008, 2010; Izotov et al. 2016b, 2018a; Flury et al. 2022b; Saldana-Lopez et al. 2022; Jaskot et al. 2024a; Chisholm et al. 2022). These signposts have been used as indirect tracers of escaping LyC emission and have been combined recently into a multivariate indicator of LyC escape (Jaskot et al. 2024a,b).

It is imperative to consider the physical conditions that facilitate the escape of sufficient ionizing photons into the IGM, and result in the observed correlations discussed above (e.g. as discussed in Steidel et al. 2018; Gazagnes et al. 2020; Saldana-Lopez et al. 2022; Flury et al. 2022b). Hot massive stars, the primary source of the ionizing radiation, reside in extremely gas rich regions in star forming galaxies with a very high Hydrogen column density (10^{21} to 10^{24} cm $^{-2}$). This is roughly 4 to 7 orders of magnitude higher than the HI column density required to produce optical depth of unity at the Lyman edge ($\sim 10^{17}$ cm $^{-2}$). Thus extreme conditions in the interstellar medium (ISM) are necessary for a significant fraction of the ionizing flux to escape the IGM. One possible scenario is that ionizing radiation field from intense star forming regions can almost fully photoionize the surroundings, and thus can create channels of ionized gas that enables the escape of LyC photons. This “density-bounded nebula” picture is consistent with higher LyC escape found in galaxies with higher ionization, strong nebular emission lines, and low stellar masses with intense starburst activities.

In contrast, Borthakur et al. (2014) and Wang et al. (2019) found four galaxies which appear to be an entirely different class of LyC leaking sources. These galaxies exhibit properties entirely different from the traditionally known LCEs and are characterized by large stellar mass $> 10^{10} M_{\odot}$, a much lower ionization state ($[\text{OIII}]/[\text{OII}] \sim 1$), with the UV emission dominated by an extremely compact (few hundred parsecs) central region. They also display a relative weakness of $[\text{SII}]6717\text{\AA}$, 6731\AA lines defined with respect to typical star forming galaxies. It has been argued that a different mechanism may be at play here: these massive and compact starbursts drive extreme galactic winds, which blow holes and clear out low density channels in the neutral ISM through which LyC photons can escape (e.g., Bergvall et al. 2006; Heckman et al. 2011). In a classical HII region, a $[\text{SII}]$ deficiency indicates a depleted partially ionized region near the outer edge of the Stromgren sphere (Pellegrini et al. 2012; Borthakur et al. 2014; Heckman et al. 2011; Alexandroff et al. 2015). In the massive, compact leaky galaxies this is possibly due to the fully ionized channels created by the feedback driven outflows.

Thus, there may be two different mechanisms to create channels in the ISM to enable LyC escape. In this study, we expand the second sample of members of the massive,

compact leaky starbursts by observing five new candidates using HST/COS observations. These galaxies are selected to be [SII]-deficient, massive star forming galaxies (selection criteria further described in §2). We use COS G140L observations that reach below the Lyman Limit to directly measure the amount of escaping LyC radiation, and to derive the LyC escape fraction. We also study the LyC escape fraction and the nature of correlations with host galaxy properties, and compare the properties of this population of galaxies with the traditional LCEs from the LzLCS survey (Flury et al. 2022a,b; Saldana-Lopez et al. 2022). Our main goal is to determine whether there exist a real dichotomy in the properties of the leaky galaxies in these two classes, and how this may depend on the physical condition of the host galaxy and its ISM.

The structure of the paper is as follows. In §2, we summarize the sample selection for this study. §3 discusses the data acquisition, reduction, and analysis techniques. In §4, we present the results and assess their significance in the context of the existing literature for Lyman continuum emitters. Finally, we summarize our conclusions in §5.

2. SAMPLE SELECTION

In this study, we investigate a new class of LyC leaky galaxies, selected based on the relatively weak emission of [SII] 6717 Å, 6731 Å lines compared to those typically observed in star-forming galaxies. Additionally, these galaxies are characterized by compact host galaxies with high stellar masses. This selection criterion is designed to expand the sample of massive leaky starburst galaxies, as previously identified by Borthakur et al. (2014) and Wang et al. (2019). Thus, as part of the HST program GO 17220 (PI: T. Heckman), we observed a sample of five galaxies selected from SDSS DR12, WISE near-IR photometry, and GALEX GR6 catalogs based on the following criteria:

1. The SDSS optical spectrum is dominated by starburst activity, showing no indication of an AGN. This is based on the line ratios aligning with ionization from young, hot stars, as indicated by the standard Baldwin, Phillips & Terlevich (BPT) diagnostic diagram (Baldwin et al. 1981). There is an absence of emission lines commonly associated with AGN activity, such as [NeV] and He II, and the Balmer line profiles do not exhibit broad wings.
2. An estimated far-UV flux inside the COS aperture $> 10^{-16}$ erg cm⁻² s⁻¹ Å⁻¹ at rest frame 1000 Å.
3. An [SII]-deficiency (or Δ [SII]) of at least 0.2 dex relative to the normal star-forming galaxies, defined by the distance from the star formation ridge (Kewley et al. 2001) in the [SII]-BPT. A detailed explanation of the method of calculation of Δ [SII] is given in §3.3. As shown by Wang et al. (2019), the relative weakness of the [SII] emission lines is a strong indirect tracer of the leakage of Lyman-continuum emission.
4. Redshifts higher than 0.25. This ensures that the Lyman Continuum region falls at wavelengths over which the COS has high sensitivity (>1150 Å).
5. A seeing-de-convolved half-light radius of $<0.5''$ (typically < 2 kpc) based on SDSS u-band images. This mimics the small sizes of galaxies in the epoch of reionization, and ensures that the majority of light is captured within the COS aperture.
6. Stellar mass $> 10^{10} M_{\odot}$ to select massive galaxies (Thomas et al. 2013).

The COS NUV acquisition images of the sources are shown in Fig. 1. The targets and their relevant properties are listed in Table. 1.

Throughout the study, we use the term "massive leakers" to refer to the combined sample of 5 sources from this work, the three massive, [SII]-deficit LyC leakers previously studied in Wang et al. (2019) and the massive LyC leaker from Borthakur et al. (2014). We compare these massive leaker population with the more traditional LCE sample from the low-z Lyman continuum leaker survey (LzLCS: Flury et al. 2022a; Saldana-Lopez et al. 2022). The LzLCS sample includes 66 candidate low redshift ($z \sim 0.3-0.4$) leakers selected from SDSS & GALEX data archive. The sample spans a broad range in host galaxy parameters like [OIII]/[OII], Σ_{SFR} , stellar mass, metallicity, UV slope and others. The program was carried on with 134 orbits of HST/ COS spectroscopy a part of GO 15626 (Cycle 26, PI: A. Jaskot). All the measurements of host galaxy properties of the LzLCS sample are obtained from the catalog presented in Flury et al. (2022a,b). In addition to the 66 LzLCS galaxies, the catalog also compiles the measurements of 23 other LCE candidates from the literature observed by HST/COS as part of other programs (Izotov et al. 2016b,a, 2018a,b, 2021). The HST/COS observations were reprocessed and the LyC fluxes were recomputed systematically by Flury et al. (2022a) to obtain consistent LyC measurements. We will refer to this combined sample of 89 galaxies as our comparison sample, and often loosely as the LzLCS+ sample (since it includes other LCEs in addition to the LzLCS survey).

3. DATA ACQUISITION AND ANALYSIS

3.1. Processing HST/COS observations

The 12 orbits of HST COS spectroscopy utilized in this study were obtained through the observing program GO 17220 (PI Timothy Heckman). The G140L grating was used

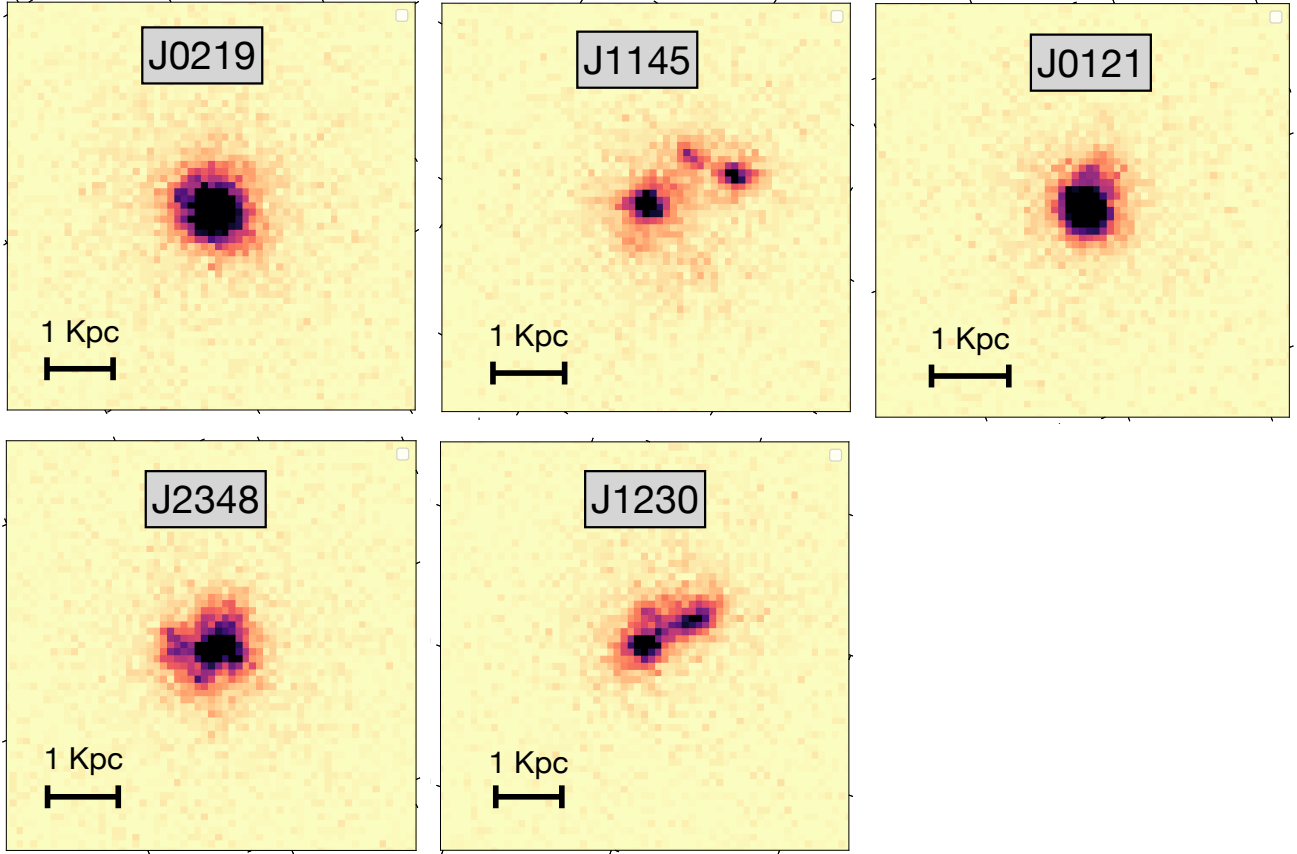


Figure 1. COS near-UV acquisition images of the five [SII]-weak selected targets in this work: (a) J0219 (nonemitter), (b) J1145 (LCE), (c) J0121 (LCE), (d) J2348 (nonemitter), and (e) J1230 (LCE). The images are $1.2''$ by $1.2''$ in angular scale. The bar in the bottom left indicates a physical scale of 1 Kpc at the target’s redshift.

Table 1. The Lyman Continuum escape fraction and host galaxy properties of the five massive leakers presented in this work.

ID	z	$\frac{F_{900}}{F_{1100}}$	$f_{\text{esc,HI}}$	$f_{\text{esc,tot}}$	[OIII]/[OII]	$H\beta$ EW [Å]	$Ly\alpha$ EW [Å]	$E(B-V)_{\text{UV}}$	$12 + \log(O/H)$	$\text{Log}_{10}M_{\star}$ [M_{\odot}]	SFR_{UV} [$M_{\odot} \text{ yr}^{-1}$]	$\Sigma_{\text{SFR,UV}}$ [$M_{\odot} \text{ yr}^{-1} \text{ kpc}^{-2}$]	$\Delta[\text{SII}]$
J0121	0.264	0.17	0.713	0.0043	0.515	21	43	0.298	8.59	10.5	60	130.9	-0.278
J0219	0.327	<0.017	<0.05	<0.0035	0.52	13	8	0.235	8.48	10.5	26	22.1	-0.457
J1145	0.287	0.221	0.841	0.0264	0.490	26	< 1	0.345	8.48	10.0	25	6.7	-0.249
J1230	0.342	0.078	0.333	0.011	0.437	18	11	0.30	8.49	10.4	36	13.5	-0.213
J2348	0.313	<0.022	<0.14	<0.0025	0.607	16	32	0.351	8.53	10.6	53	31.4	-0.169

at 800 \AA in COS Lifetime Position 4, covering an observed wavelength range of $800\text{-}1950 \text{ \AA}$. At the median redshift of our sample, this corresponds to a rest-frame wavelength range of approximately $615\text{-}1500 \text{ \AA}$. The spectral resolution of the obtained spectrum $R \sim 1050$ at 1100 \AA . The COS spectroscopic aperture has a field of view of diameter $2.5''$ and is centered based on the NUV acquisition images taken as part of the program.

We retrieved the COS data from the MAST archive and processed the raw spectra using a combination of standard

(CALCOS¹) and custom software (FAINTCOS²; Worseck et al. 2016; Makan et al. 2021) to best model the background and optimize the measurement of the LyC. We reduced the data following the method described in Flury et al. (2022a). The major component of the data reduction is accurately subtracting the dark counts and the background signal, which can contribute significantly to the flux in the LyC region. So

¹ <https://github.com/spacetelescope/calcos>

² <https://github.com/kimakan/FaintCOS>

we take a few additional steps to mitigate the challenge. We describe them briefly below.

The charge produced by the amplifying microchannel plate in the COS detector is measured by the ‘‘pulse height amplitude’’ (PHA). The PHA values are triggered by science events, and also spuriously by dark current and geomagnetic activity. This often extends the PHA distribution well beyond the possible values of science events (Worseck et al. 2016; Izotov et al. 2016a). So, following Flury et al. (2022a), we screen the PHA values and include only values within the permitted 1-12 range for lifetime position 4, to mitigate dark current and other background effects without excluding science events.

We then process the data through the standard COS pipeline `Calcos`, version 3.4.7. `CALCOS` performs the standard reduction steps including flat-fielding, deadtime corrections, wavelength, and flux calibrations. We turn off the native background correction in `Calcos` and instead subtract a custom super-dark image following the procedure in Leitherer et al. (2016); Wang et al. (2019); Flury et al. (2022a). A unique super-dark image is created for every science target by combining all the HST/COS dark frames taken within ± 1 month of the observing time of the target and computing the average. The ± 1 month window is taken to minimize the effects of temporal fluctuations of the dark current. We use the custom software package `FAINTCOS` to estimate the dark current model from the chosen frames and implement the background subtraction to the science spectra. The package computes, for each observation, the cumulative PHA distribution of the chosen dark current observations and matches them with science background images via the Kolmogorov-Smirnoff test. To ensure that the super dark image technique has been successful, we compare the spatial variation of the dark model to the science image background and find that they agree reasonably well. `Faintcos` also estimates the contamination from scattered geocoronal Ly α background from Worseck et al. (2016) model, coadds individual science exposures for each object, and bins them to Nyquist-sample the G140L resolution of ~ 1.1 Å. The final spectra for our 5 sources, shown in Fig. 2, are now ready for the next steps of analysis.

3.2. Measuring Lyman Continuum

We smooth the spectra of all sources with a Gaussian kernel with full width at half maximum of about 1.0 Å, to achieve the native resolution and boost the relatively low signal-to-noise. We measure the LyC flux in each source in a rest frame 20 Å window as close as possible to $\lambda_{\text{rest}} = 900$ Å, while simultaneously avoiding contamination from Ly α and NI $\lambda 1200$ geocoronal emission lines. Thus, we avoid wavelengths above $\lambda_{\text{obs}} = 1180$ Å (similar to Flury et al. 2022a). We also do not choose the spectral range to include

wavelengths below $\lambda_{\text{obs}} = 1100$ Å, since the sensitivity of the G140L grating and the signal-to-noise of the spectra decline rapidly. Thus, to compute LyC flux ($F_{\lambda_{\text{LyC}}}$) for our sources at $z = 0.26 - 0.34$, we compute the mean background subtracted flux density in the chosen 20 Å spectral window generally within $\lambda_{\text{rest}} = 860-910$ Å, such that the above conditions are met. This ensures a uniform measurement of the LyC flux $F_{\lambda_{\text{LyC}}}$ across our entire sample and is also consistent with the LzLCS survey to enable direct comparison.

One of the main goals of this investigation is to explore the roles of both dust extinction and absorption by HI in determining the fraction of escaping LyC photons. We also want a mix of indicators that includes a simple model-independent parameter. We will therefore characterize the escape of LyC photons by reporting three different quantities: 1) The direct flux ratio $F_{\lambda_{\text{LyC}}}/F_{\lambda 1100}$ (often labelled as F_{900}/F_{1100}) 2) $f_{\text{esc,tot}}$ the ratio of $F_{\lambda_{\text{LyC}}}$ to the intrinsic contribution from the stars, as inferred from fitting models of the observed UV continuum (often labelled as absolute escape fraction $f_{\text{esc,abs}}$), and 3) $f_{\text{esc,corr}}$ (often labelled as $f_{\text{esc,HI}}$), which is corrected for the effects of dust attenuation and represents the fraction of LyC photons that would escape after surviving neutral hydrogen absorption, assuming no dust is present.

To derive $F_{\lambda_{\text{LyC}}}/F_{\lambda 1100}$, we transform the observed spectra to the rest frame of the galaxy using SDSS spectroscopic redshifts. We compute $F_{\lambda_{\text{LyC}}}$ by calculating the mean flux density in the LyC spectral window of width 20 Å, as discussed above. $F_{\lambda 1100}$ is calculated by taking average flux in $1090 < \lambda_{\text{rest}} < 1100$ Å, i.e. keeping the spectral window width to be the same as the LyC flux for consistency. Our method is consistent with previous studies, allowing for direct comparison (Wang et al. 2019; Flury et al. 2022a).

We estimate $f_{\text{esc,tot}}$ by taking the ratio of the observed flux in the LyC region and the intrinsic flux in the same wavelength range derived from the best-fit stellar model spectra. The stellar continuum modeling is performed using a customized PYTHON script `FICUS`³, which stands for *F*itting *t*he *s*tellar *C*ontinuum of *U*V *S*pectra (Saldana-Lopez et al. 2022; Chisholm et al. 2019). The continuum modeling is achieved in `FICUS` by fitting every observed spectrum with a linear combination of multiple bursts of single-age and single-metallicity stellar population models and performing a chi-squared minimization. By default, `FICUS` inputs the fully theoretical `STARBURST99` single-star models without stellar rotation (SB99; Leitherer et al. 2011, 2014) using the Geneva evolution models (Meynet et al. 1994), and computed with the `WM-BASIC` method (Pauldrach et al. 2001; Leitherer et al. 2010). The SB99 models assume a Kroupa

³The `FICUS` code is publicly available here: <https://github.com/asalda/FICUS.git>

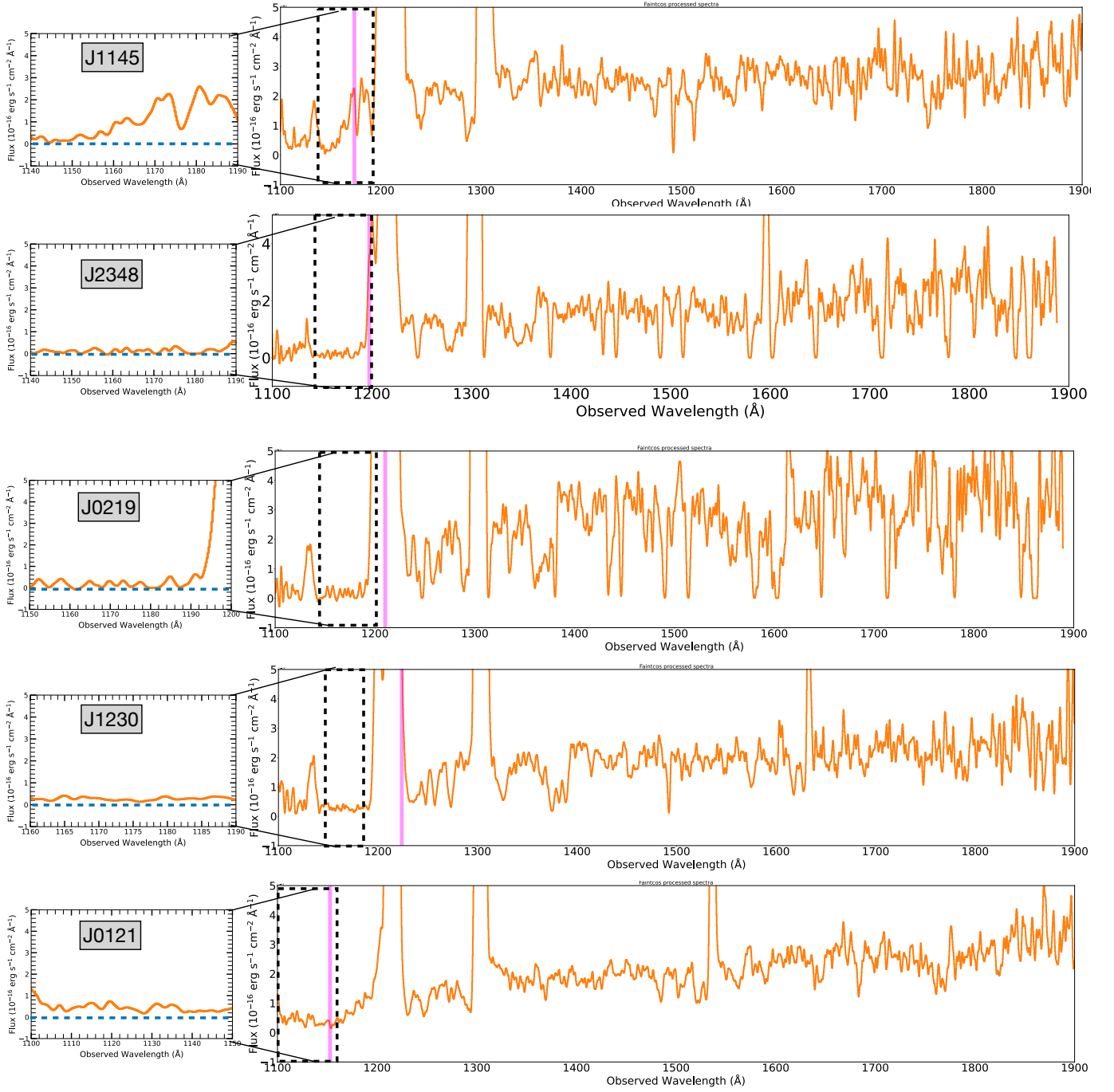


Figure 2. HST/COS spectra (orange) of the five sources analyzed in this work. The left panels show the spectral region around the LyC edge, while the right panels show the full spectra. The gray shaded region indicates the 1σ uncertainty in flux density. The location of the Lyman limit at the redshift of the source is indicated by the vertical magenta line. The blue dashed lines in the left panel show the zero flux level. Geocoronal emission from telluric Ly α is clipped in the spectra.

(2001) initial mass function (IMF) with a high-(low-)mass exponent of 2.3 (1.3), and a high-mass cutoff at $100 M_{\odot}$. The spectral resolution of the SB99 models is $R \sim 2500$, and it remains approximately constant at FUV wavelengths. Four different metallicities (0.05, 0.2, 0.4, and $1 Z_{\odot}$) and ten ages for each metallicity (1, 2, 3, 4, 5, 8, 10, 15, 20, and 40 Myr) were chosen as a representative set of 40 models for our UV spectra. Finally, a nebular continuum was generated by self-consistently processing the stellar population synthesis models through the CLOUDY V17.0 code 4 (Ferland et al. 2017), assuming same gasphase and stellar metallicities, an ionization parameter of $\log(U) = -2.5$, and a volume hydrogen density of $n_{\text{H}} = 100 \text{ cm}^{-3}$ (Chisholm et al. 2019).

To perform the fitting, the observed spectra are first manually placed into the rest-frame by multiplying by the corresponding $1/(1+z)$ factor. Both the spectra and the models were then normalized by the median flux within a wavelength interval free of stellar and ISM features (1350–1370 Å), and all the fits are performed in the same rest-wavelength range (930–1425 Å). Finally, the models are convolved by a Gaussian kernel to the instrumental resolution ($R \sim 1000$). The best-fit stellar model spectrum for each source is integrated over the optimal 20 Å wide LyC spectral window to estimate the modeled (i.e. intrinsic) LyC flux. Fig. 3 shows the FICUS fitting for one of the galaxies (ID: J0121, at $z = 0.264$), with the observed spectrum in black and fitted stellar continuum in red.

We use FICUS for stellar continuum modeling to be consistent with the results from the LzLCS+ study. However, for one of our sources (ID: J1145), the FICUS fit fails due to inadequate signal to noise, particularly at the red end of the spectrum. So for J1145, we directly generate a grid of synthetic spectra from SB99 models, and assume a continuous and constant star formation rate (SFR) = $1 M_{\odot}$, and a Kroupa Initial mass function (Kroupa 2001). We generate a total of eight sets of SB99 models based on two choices each for burst age (10^7 and 10^8 yr), metallicity (solar or $1/7$ solar), and whether or not stellar rotation is present. We assume the stellar population evolves from the zero-age main sequence using the evolutionary models of the Geneva Group (similar to the FICUS assumptions). The model spectra are interpolated into the same wavelength array as its corresponding COS spectrum, convolved with the same Gaussian kernel, and normalized to the common flux level (1350–1370 Å) – following the same procedure as the rest of the sources. The best fit is chosen by eye; more specifically, we closely examine the match of the two strong stellar wind features – O VI 1032,1038 and N V 1238,1242 (similar to Wang et al. 2019). These P-Cygni features trace the most massive stars that are responsible for producing most of the ionizing continuum. We multiply the SB99 model-derived LyC flux with the total SFR since the stellar models were assumed to have

a constant SFR = $1 M_{\odot}/\text{yr}$ in the model grid. The SFR was derived using WISE band 3 and band 4 data to estimate a rest-frame 24 micron luminosity and then using the relationship in Kennicutt & Evans (2012) to get SFR_{IR}. We can then use this SFR and the SB99 model to obtain the intrinsic LyC flux ($F_{\lambda\text{LyC,int}}$).

Then $f_{\text{esc,tot}}$ is essentially the ratio of $F_{\lambda\text{LyC}}/F_{\lambda\text{LyC,int}}$. The measured value of this escape fraction then depends on both the effects of dust extinction and photoelectric absorption of the LyC due to hydrogen.

For method 3, we measure the dust-corrected escape fraction $f_{\text{esc,corr}}$ which is the ratio of emergent LyC flux after removing the effects of dust extinction compared to the intrinsic flux. To determine the amount of dust extinction, we first measure the rest-frame 1500 Å flux and convert that to luminosity. We use the L_{1500} to estimate SFR_{UV} using the Kennicutt & Evans (2012) relation, and derive the attenuation at 1500 Å by:

$$A_{1500} = 2.5 \times \log_{10}(\text{SFR}_{\text{IR}}/\text{SFR}_{\text{UV}}) \quad (1)$$

The far-UV dust attenuation law from Reddy et al. (2016) suggests that $E(B-V)_{900} = 0.226 \times A_{1500}$, extrapolated from 950 to 900 Å based on their fit to data between 950 and 2000 Å. The dust-corrected ratio $F_{\lambda\text{LyC}}/F_{\lambda1100,\text{corr}}$ is calculated using $10^{0.4 \times 0.226 \times A_{1500}} \times F_{\lambda\text{LyC}}/F_{\lambda1100}$. The final f_{esc} estimate is obtained by dividing the dust-corrected $F_{\lambda\text{LyC}}/F_{\lambda1100,\text{corr}}$ by the intrinsic $F_{\lambda\text{LyC}}/F_{\lambda1100,\text{int}}$ derived from the modeled spectrum. This f_{esc} value measures only the photoelectric absorption of LyC photons by HI in the absence of dust, providing complementary information to $f_{\text{esc,tot}}$. Throughout the text, $f_{\text{esc,corr}}$ is also referred to as $f_{\text{esc,HI}}$.

3.3. Measurement of ancillary parameters

This paper aims to study the LyC escape fraction and its dependence on host galaxy properties compared with the LzLCS survey. Here we list the ancillary parameters we measure.

We measure the equivalent width (EW) of the Ly α emission line from the extracted COS spectra. The continuum is modeled by fitting a linear function to the continuum within a spectral window of $\pm 30\text{Å}$ on either side of the emission line using an iterative sigma clipping technique to exclude noise spikes. To measure Ly α EW, the observed spectrum is normalized by dividing the spectrum by the modeled continuum and then corrected for redshift. All measured fluxes and EWs of the rest-frame optical emission lines are taken from the Sloan Digital Sky Survey (SDSS) spectral data, specifically from the value-added catalog provided by the Portsmouth group (Thomas et al. 2013). A signal-to-noise ratio (S/N) cut of 5 is imposed for any emission line detection. The flux values for [OIII]5007 and [OII]3726, 3729Å emission lines are obtained from the catalog to compute the [OIII]/[OII] ratio.

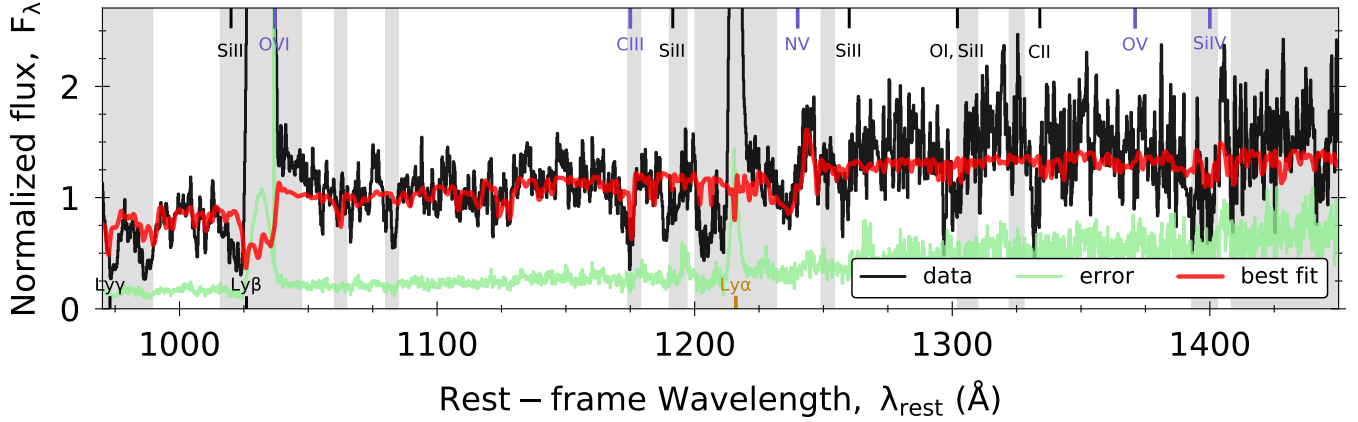


Figure 3. SED fitting results for galaxy J0121 with FICUS. The observed and error spectra are displayed in black and light green. The best-fitting stellar continuum is overplotted in red, while the spectral regions masked during the fit are shown in grey. The spectrum, shown in F_λ units, has been normalized over 1350–1370 Å. The most prominent stellar features, nebular and ISM absorption lines are indicated with black vertical lines at the top part of the figure.

These are dusty systems, so our primary measure of SFR is SFR_{IR} from the WISE mid-IR photometry, as described above. We also calculated SFR_{UV} based on the observed continuum flux measured at 1500 Å (see above). We do not use a SFR based on the Balmer emission-lines since these can significantly underestimate the SFR in cases in which only a fraction of the ionizing photons are absorbed by HI in the galaxy ISM.

We measure the [S II] deficiency ($\Delta[\text{SII}]$) in a differential sense: as a quantity relative to the majority of star-forming galaxies in the SDSS survey. To do this, we first construct the BPT/VO [S II]/ $H\alpha$ versus [O III] 5007/ $H\beta$ diagnostic diagram (Baldwin et al. 1981; Veilleux & Osterbrock 1987) for our objects using the flux values from the Portsmouth catalog (Thomas et al. 2013). We then subtract the measured [SII]/ $H\alpha$ from the mean BPT/VO relation derived for a large sample of SDSS star-forming galaxies from Wang et al. (2019). Thus, we define the [SII] deficiency as a galaxy’s displacement in $\log([\text{SII}]/H\alpha)$ from the Wang et al. (2019) polynomial fit to the mean star-forming relation, as follows:

$$y = -0.487 + 0.014\xi + 0.028\xi^2 - 0.785\xi^3 - 3.870\xi^4 + 0.446\xi^5 + 8.696\xi^6 + 0.302\xi^7 - 6.623\xi^8$$

where ξ is $\log([\text{OIII}]/H\beta)$ and y is $\log([\text{SII}]/H\alpha)$. Thus, $\Delta[\text{SII}] = \log([\text{SII}]/H\alpha)_{\text{observed}} - y$

We use the COS near-UV images to compute the half-light radius for a given galaxy. All targets are located well within the COS aperture radius of 1.2". We accounted for the vignetting of the COS aperture, where the effective radius of the aperture diminishes to $\sim 0.4''$, while calculating the half light radius. We estimate the background signal from the mean of an annulus of $r_{\text{in}} = 0.9''$ and $r_{\text{out}} = 1.1''$. The half-light radius is calculated by determining a circle that encloses

half of the total near-UV emitted light in the background subtracted image within the 0.4" vignetted aperture.

Finally, the oxygen abundance of the interstellar medium (ISM) is calculated from the strong emission line tracers following Pettini & Pagel (2004):

$$12 + \log_{10}(\text{O}/\text{H}) = 8.73 - 0.32 \times \text{O3N2} \quad (2)$$

where $\text{O3N2} = \log_{10} \frac{[\text{OIII}]\lambda 5007/H\beta}{[\text{NII}]\lambda 6584/H\alpha}$. The relation is valid for $-1 < \text{O3N2} < 1.9$ and is insensitive to dust extinction. Note, for the LzLCS+ sample, the oxygen abundance is calculated from the [OIII] $\lambda 4363$ Å line.

4. RESULTS & DISCUSSIONS

4.1. LyC escape fraction

We detect a significant flux in the LyC region below the Lyman edge for 3 out of our 5 galaxies. For these three detected sources, we report the mean background-subtracted flux density in the LyC spectral window (as explained in §3.2). In case of non-detections, we take the 84th percentile of the background distribution to be the upper limit on $F_{\lambda\text{LyC}}^{\text{obs}}$ following Flury et al. (2022a). To confirm the LyC detections, we examine the cross-dispersion profiles of the two-dimensional spectra of our sources in the LyC window and compare with the non-ionizing stellar counterpart centered at $\lambda_{\text{rest}} \sim 1100$ Å. Fig. 4 shows example profiles for a LyC detected and non-detected source.

For the LyC detected sources, we report flux densities ($F_{\lambda\text{LyC}}$) of $5.38 \times 10^{-17} \text{ erg cm}^{-2} \text{ s}^{-1} \text{ \AA}^{-1}$ for J1145, $2.9 \times 10^{-17} \text{ erg cm}^{-2} \text{ s}^{-1} \text{ \AA}^{-1}$ for J0121, and $1.58 \times 10^{-17} \text{ erg cm}^{-2} \text{ s}^{-1} \text{ \AA}^{-1}$ for J1230. For the other two sources, we report upper limits. The values are listed in Table. 1. Fig. 5 shows the observed LyC flux vs. redshift for the massive leakers sample (see §2 for the sample definition). Yellow square denote sources from this work, while yellow diamond

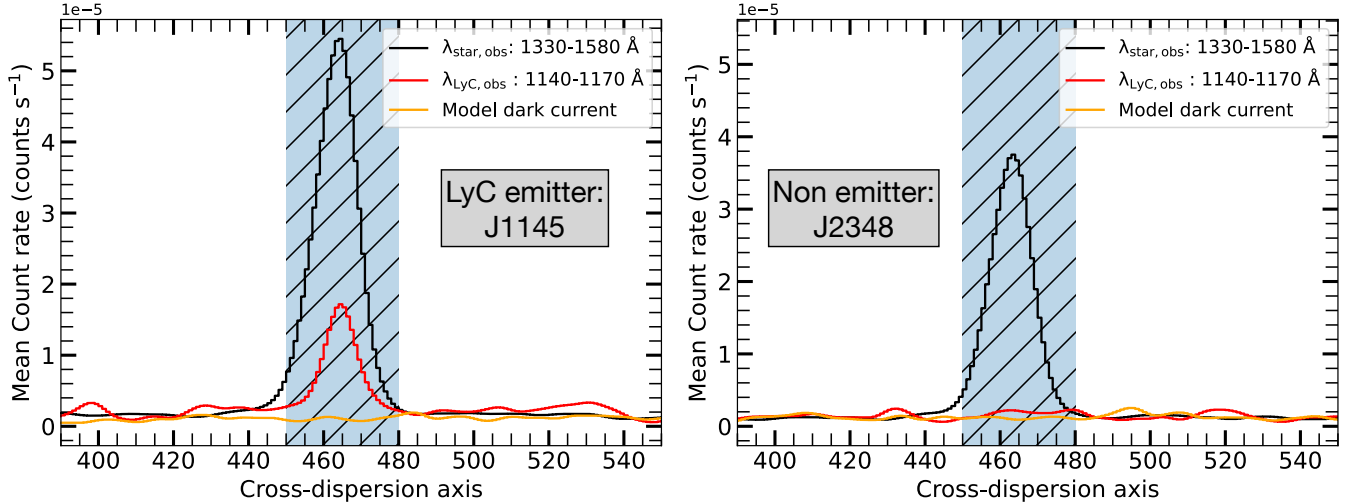


Figure 4. Example spatial cross section of the two-dimensional spectrum for a well-detected Lyman Continuum Emitter (left) and a nonemitter (right) from this work. The black line represents the nonionizing starlight continuum, the yellow line represents the model dark current, red line represents the LyC counts, and the blue hatched stripe represents the spectral extraction aperture.

represent Wang et al. (2019) and Borthakur et al. (2014) objects, compared with LzLCS+ objects in blue circles (Flury et al. 2022b).

As mentioned in §3.2, we report three different ways to measure the escape fraction. The first and the simplest method is the ratio of the observed fluxes in the LyC region to that of rest wavelength of 1100 Å $F_{\lambda_{\text{LyC}}}/F_{\lambda_{1100}}$. The rest-frame 1100 Å flux provides a measurement for the non-ionizing stellar continuum, and thus, the mean ratio of LyC to 1100 Å is an indirect proxy for f_{esc} . It is very useful since it is directly derived from observed spectrum in a model-independent way without any assumptions about stellar populations or other galaxy properties.

Fig. 6 shows the histogram of f_{esc} measured from three different methods as described in §3.2 in three panels. The left panel shows the distribution of $F_{\lambda_{\text{LyC}}}/F_{\lambda_{1100}}$ for the massive leakers population (blue) and LzLCS+ sample (red). The mean $F_{\lambda_{\text{LyC}}}/F_{\lambda_{1100}}$ for the massive leakers which are LyC detected = 0.17, compared to a mean value of 0.05 obtained from the LzLCS+ sample. The three LyC detected sources from this study exhibit a mean $F_{\lambda_{\text{LyC}}}/F_{\lambda_{1100}}$ to be 0.12, which is a factor of 2 higher than the Flury et al. (2022a) sample.

$F_{\lambda_{\text{LyC}}}/F_{\lambda_{1100}}$ is directly observable, but is sensitive to a number of factors in addition to the LyC escape fraction, including dust attenuation, SFR, metallicity, and burst ages – complicating its interpretation. Hence, we computed two other estimates of f_{esc} as described in §3.2. There are two main sources of opacity provided by the galaxy ISM which play a primary role in deciding what fraction of LyC photons can escape into the IGM. The first source of opacity is photoelectric absorption due to neutral Hydrogen, which produces a rapid drop in flux density at the Lyman edge. The second is dust. Dust absorption suppresses the flux by a smoothly

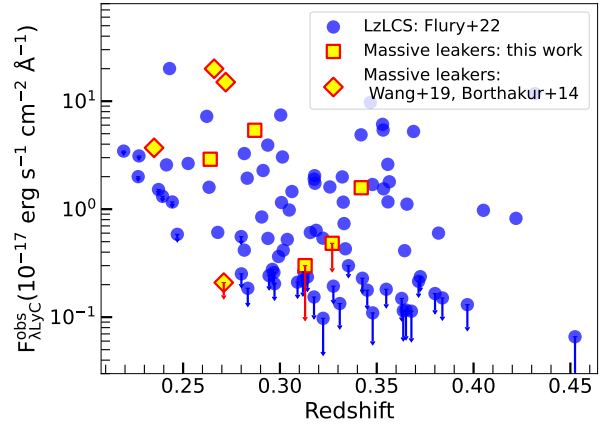


Figure 5. LyC measurements from this study (diamonds) alongside published data from Wang et al. (2019) and Borthakur et al. (2014) (squares) for the massive leaker population observed with HST/COS. Upper limits are indicated for LyC non-emitters. Measurements from the combined LzLCS+ published sample from Flury et al. (2022a) are represented by circles.

varying function that increases with decreasing wavelength, thus making UV flux susceptible to its effects. However, it doesn't produce any sharp change in flux around the Lyman edge.

To consider the escape fraction due to the effect of both photoelectric absorption and the presence of dust, we use method 2, i.e. measuring $f_{\text{esc,tot}}$. It involves the ratio between the observed flux in the LyC region to the intrinsic flux from the non-ionizing stellar counterpart derived from stellar population models to provide a measure of the fraction of the LyC photons that suffer both photoelectric absorption by atomic hydrogen as well as dust absorption in the ISM. This yields $f_{\text{esc,tot}} = 0.0264, 0.0043, \text{ and } 0.011$ for

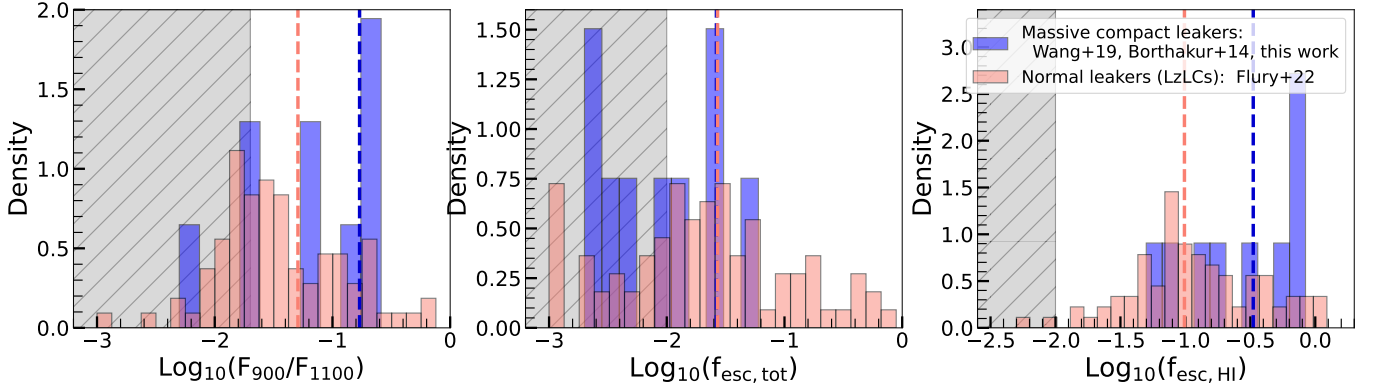


Figure 6. Histogram distributions of three different estimates of LyC escape fraction (as detailed in §3.2) for the combined massive leaker population from this work, Wang et al. (2019) and Borthakur et al. (2014) (blue), alongside the LzLCS+ sample from Flury et al. (2022a) (red). The left panel displays the $F_{\lambda_{\text{LyC}}}/F_{1100}$ values derived from direct flux ratios (method 1), the middle panel shows the distribution of $f_{\text{esc,tot}}$ obtained from stellar model fits to the observed UV continuum (method 2), and the right panel presents $f_{\text{esc,HI}}$ estimates representing LyC escape due to HI absorption only in the absence of dust (method 3). The mean of the LyC-detected sources are indicated by dashed vertical lines (red: LzLCS+ sample, blue: massive leakers). The gray-shaded hatched region shows the non-emitters with upper limits.

J1145, J0121 and J1230. The estimated escape fractions are thus rather small. The upper limits for the remaining two non-detected sources are 0.0025 and 0.0035 for J2348 and J0219 respectively. Fig. 6 middle panel shows the comparison of $f_{\text{esc,tot}}$ distribution between LzLCS+ and the massive leakers. The detected massive leakers exhibit a mean $f_{\text{esc,tot}} \sim 0.0264$ (shown by blue vertical line) – remarkably similar to the detected LzLCS+ sample (mean $f_{\text{esc,tot}} \sim 0.027$).

In the final step (method 3), we correct these estimates for the effect of dust absorption, to derive an estimate of how much of the LyC photons would escape only considering photoelectric absorption by hydrogen. The difference in estimates between method 2 and 3 enables us to isolate the effect of neutral Hydrogen and dust absorption on LyC escape fractions. We employ the method described in §3.2 to determine $f_{\text{esc,HI}}$ (or $f_{\text{esc,corr}}$), i.e. the f_{esc} determined by photoelectric absorption by hydrogen only. We obtain $f_{\text{esc,corr}} = 0.841, 0.583$ and 0.363 for J1145, J0121 and J1230, with a considerably high mean value of 0.59. We calculated $f_{\text{esc,corr}}$ for the LzLCS+ sample using a method consistent with our own analysis and found a mean $f_{\text{esc,corr}}$ of 0.2 for the LzLCS+, which is approximately three times lower than that of the massive leakers identified in this study. This indicates that a large fraction of LyC photons in these massive leakers could escape from the ISM after considering photoelectric absorption, but they eventually get absorbed by the dust, resulting in much lower escape fractions. Fig. 6 show a higher value of F_{900}/F_{1100} and also $f_{\text{esc,HI}}$ in massive leakers on average than the LzLCS+ population. However, their $f_{\text{esc,tot}}$ is significantly suppressed and is almost equal to LzLCS+ detected sources, and that originates due a higher amount of dust attenuation.

To directly assess the relative impact of photoelectric absorption by neutral hydrogen and that of dust on the LyC escape fraction (similar to Xu et al. 2023), we calculate the

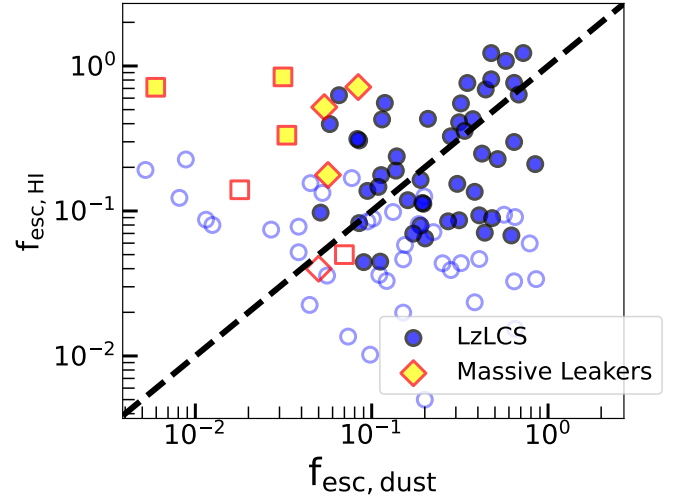


Figure 7. The fraction of LyC photons escaping into the IGM is determined by two main factors: HI absorption and dust attenuation. Here, LyC escape fractions considering only HI absorption $f_{\text{esc,HI}}$ are compared with those considering only dust attenuation $f_{\text{esc,dust}}$ for the LzLCS+ sample (circles; Flury et al. 2022a) and massive leakers (squares: this study, diamonds: literature sample from Wang et al. 2019; Borthakur et al. 2014). Hollow symbols represent upper limits for non-emitters. The solid line indicates a one-to-one correspondence between the two f_{esc} estimates. Most massive leakers lie above this line, with $f_{\text{esc,HI}} > f_{\text{esc,dust}}$, suggesting their LyC escape fractions would be higher if not significantly reduced by dust attenuation, unlike the LzLCS+ leakers.

escape fraction attributed solely to dust attenuation: $f_{\text{esc,dust}} = \frac{f_{\text{esc,tot}}(\text{Method 2})}{f_{\text{esc,HI}}(\text{Method 3})}$. Fig. 7 illustrates the difference between the escape fractions due to dust ($f_{\text{esc,dust}}$) and neutral hydrogen ($f_{\text{esc,HI}}$). Most massive leakers have $f_{\text{esc,HI}} > f_{\text{esc,dust}}$, indicating that their LyC escape fractions are significantly reduced by dust attenuation.

4.2. Comparison with other indirect f_{esc} diagnostics

The LzLCS survey and other studies in the past have shown that the LyC escape often exhibits significant correlation with different host galaxy properties, albeit with substantial scatter (Wang et al. 2021; Flury et al. 2022b; Izotov et al. 2016b; Saldana-Lopez et al. 2022; Chisholm et al. 2022; Jaskot et al. 2024a). The observed correlations with f_{esc} , e.g. with SFR/Area, $f_{\text{esc}}^{\text{Ly}\alpha}$, Ly α EW, H β EW, [OIII]/[OII] (O_{32}), dust attenuation, [SII]-deficiency, β -slope and residual flux in Ly β motivated some of these quantities to be used as potential indirect signposts for f_{esc} leakage. These indirect tracers are especially important for sources where directly measuring LyC flux density is impossible, like during the EoR (e.g., Jaskot et al. 2024b). Here, we evaluate these correlations, which have been extensively explored in traditional LyC-leaking galaxies from the LzLCS+ sample, to determine their relevance to the massive leaker population. For this comparison, we use two different proxies for LyC escape in the Y-axis. Fig. 8 shows the direct flux ratio $F_{\lambda\text{LyC}}/F_{\lambda 1100}$ (or F_{900}/F_{1100}) as it is uniformly reported in previous studies and is independent of the specific method used to calculate f_{esc} . Fig. 9 shows the variation of those same quantities but with LyC escape fraction $f_{\text{esc,tot}}$ derived from stellar population modeling, which represents the total fraction of LyC photons escaping the IGM after accounting for both neutral hydrogen absorption and dust attenuation.

Fig 8 illustrates the correlations between F_{900}/F_{1100} and these different indirect tracers of LyC escape. Each panel displays the Kendall τ coefficient, indicating the strength of the correlation between the x and y values, along with the associated p-value representing the probability of the null hypothesis. Black-colored text represent the Kendall τ coefficients for the LzLCS+ sample alone, while red-colored values include both the LzLCS+ sample and the massive leakers. The results clearly show that the significance of the correlations (as indicated by τ) decreases when massive leakers are included (red) compared to the LzLCS+ sample alone (black). Visually, it is also evident that the massive leakers exhibit substantial deviations from the LzLCS+ leakers across a broad range of parameters.

The upper left panel shows the relation between F_{900}/F_{1100} and the Ly α equivalent width (EW) for the LzLCS+ sources (blue circles) and the massive leakers (yellow diamonds and squares). There is a strong positive correlation between the two quantities for the LzLCS+ sources. The Ly α line is produced from resonant scattering of Ly α photons through the line of sight, and it is plausible for it to follow f_{esc} , since both Ly α and LyC emission depend on the distribution of neutral hydrogen in a galaxy. Hence Ly α EW is often used as an indirect f_{esc} estimate (e.g., Roy et al. 2023). However, the main result here is that the massive leaker sample is shifted towards lower Ly α EW compared to the LzLCS+ galaxies.

The mean Ly α EW value for the former is 17 Å, which is 4 times lower compared with the mean Ly α EW = 70 Å from the LzLCS+ sample. The lower middle panel is an analogous plot for the H β EW. Here the massive leakers are even more strongly offset from the LzLCS+ galaxies, with much weaker H β emission.

There are several possible effects that may cause these offsets in Ly α and H β EW. First, the massive leakers have significantly higher amounts of dust extinction than the typical LzLCS+ galaxies. This could significantly reduce the amount of scattered Ly α photons that can escape. Since the amount of dust attenuation can be greater for the nebular emission-lines than for the starlight (Calzetti et al. 2000; Reddy et al. 2016) this will reduce the EW of the H β line. Second, there may be a more pronounced contribution of starlight from non-ionizing stars in the massive leakers, particularly in the optical. This will further reduce the EW of H β . Third, the F_{900}/F_{1100} values for our sources are so high that it is suppressing the amount of Balmer and Lyman photons that are intrinsically produced. Finally, the sources studied in these objects have higher stellar mass, and possibly includes a mix of old, evolved stellar population along with young stars, which can dilute the EW.

Fig 8 (upper middle panel) illustrates another key result. The LzLCS+ sample shows a positive correlation where O_{32} increases with increasing $F_{\lambda\text{LyC}}/F_{\lambda 1100}$. The simplest explanation for this positive trend between the ionization state of the ISM gas and the escape of the ionizing photons is that the column density of HI that can be photoionized is directly proportional to the ionization parameter (U - the ratio of the densities of ionizing photons and H), which is directly traced by O_{32} . This makes it more likely for fully ionized channels to be created which allow LyC escape, consistent with the proposed “density-bounded nebula” scenario. Although the dependence of O_{32} on metallicity and ionization parameter may lead to a more complicated scenario (Sawant et al. 2021; Giammanco et al. 2005; Stasińska et al. 2015), nevertheless [OIII]/[OII] is widely used as an indirect tracer of f_{esc} . However, the massive leaker sample is in striking contrast to the LzLCS+ population in this regard, with a large offset towards low O_{32} . The mean O_{32} is 0.5 which is roughly 16 times lower than the mean O_{32} observed from the the LzLCS+ sources. Thus, O_{32} doesn’t emerge as the best indirect f_{esc} estimator when the massive leakers are included. This indicates that the massive compact leakers might indeed be a separate population from the traditionally known LyC leaking galaxies with LyC escaping under entirely different ISM conditions.

The relative weakness of [SII] lines indicate a depleted (or lack of) partially ionized region in the outskirts of the Stromgren sphere of classical HII regions (Wang et al. 2019). These [SII]-weak regions trace channels that are optically

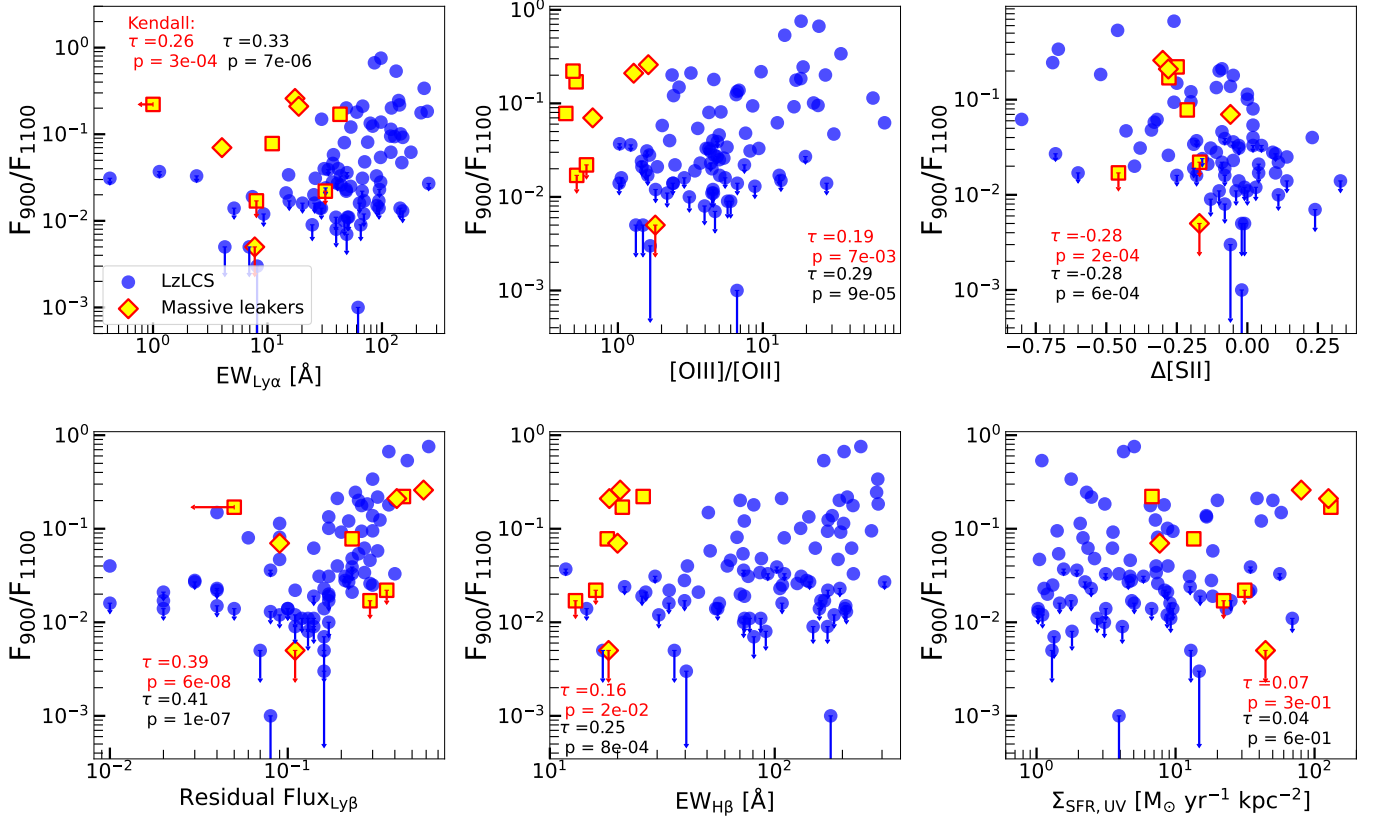


Figure 8. Correlations between f_{esc} measured from direct flux ratio: F_{900}/F_{1100} (Method 1, §3.2) and various indirect tracers of f_{esc} : Ly α equivalent width (upper left), [OIII]/[OII] ratio (upper middle), Δ [SII] (upper right), Ly β residual flux (lower left), H β equivalent width (lower middle), and star formation rate surface density (lower right). The massive leakers population from this work are shown by yellow diamonds, while those from Wang et al. (2019) and Borthakur et al. (2014) are indicated by yellow squares. The LzLCS+ sources are shown by blue circles. The objects with upper limits are denoted by the arrows. For each figure, the Kendall’s τ coefficient between the x and y values and the probability of the null hypothesis (p) are shown at the corner (red: LzLCS+ & massive leakers, black: only LzLCS+). The significance of the correlation (τ) diminishes when the massive leakers are taken into account (marked in red) compared to the correlation observed in the LzLCS+ sample only (in black). Visually, it is evident that the massive leakers deviate considerably from the LzLCS+ leakers in almost all the measured properties.

thin to ionizing radiation, thus allowing the escape of LyC photons. Fig 8 (upper right panel) shows the trend between Δ [SII] and LyC emission extends to both the LzLCS+ sample and the massive leaker population, making it a good indirect indicator of LyC escape. However, consistent with previous studies (Ramambason et al. 2020; Wang et al. 2021), the relationship shows substantial scatter, which could emerge from anisotropically escaping LyC photons, or line of sight variations, etc. Thus, even though [SII] deficiency can select LCE candidates, it is not obvious how f_{esc} can be directly derived from Δ [SII].

Fig. 8 (lower left panel) show a rather tight correlation between the residual flux (RF) in the core of the Ly β absorption-line and $F_{\lambda\text{LyC}}/F_{\lambda 1100}$. Like Δ [SII], this correlation includes both type of leakers. The mean Ly β RF for the massive leakers sample = 0.346, which is roughly two times higher than that of the LzLCS+ sample (Saldana-Lopez et al. 2022). The residual fluxes (RF) at the bottom of the HI

absorption lines are tracers of the covering fraction of the neutral hydrogen (C_f). In the case of a uniform HI screen geometry, the residual flux $\text{RF} = 1 - C_f$. As illustrated by Heckman et al. (2011), this observed trend is also consistent with picket-fence scenario where the covering factor of optically thick HI is not unity. Supernova-driven outflows or extremely intense LyC radiation (large U) can create channels or “holes” in the HI through which ionizing radiation can escape, leading to higher f_{esc} .

Finally, we show in the lower right panel the relationship between $F_{\lambda\text{LyC}}/F_{\lambda 1100}$ and the SFR per unit area (SFR/Area). Massive leakers have a high value of star formation rate surface density (SFR/Area), with values ranging between $\sim 10 - 100 M_{\odot} \text{ yr}^{-1} \text{ kpc}^{-2}$. This is typically an order of magnitude higher than the LzLCS+ leakers. The overall correlation show a significant scatter for both types of leakers.

Fig. 9 presents the same correlations as Fig. 8, but with the LyC escape fraction $f_{\text{esc,tot}}$, derived from stellar popula-

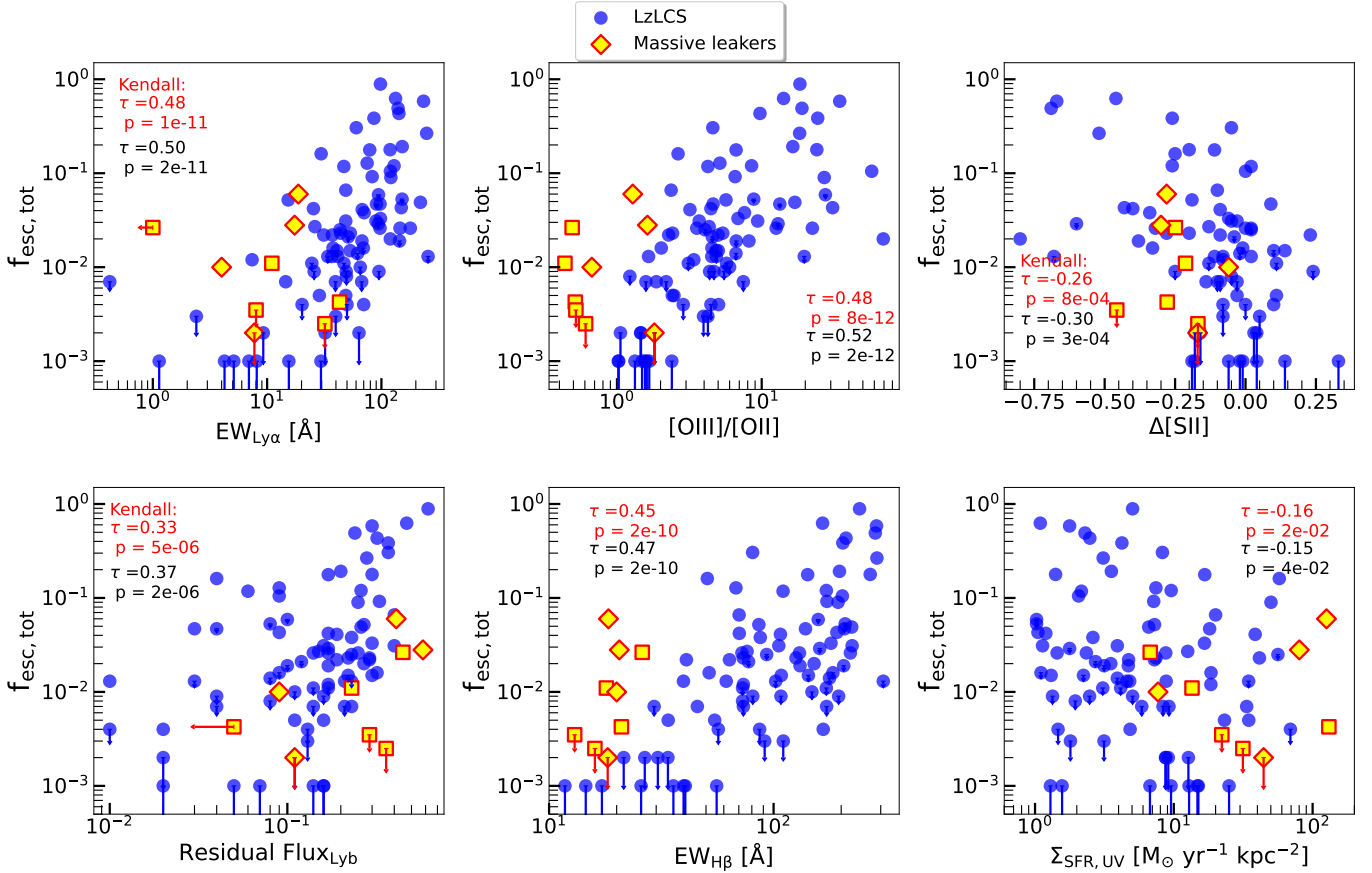


Figure 9. Correlations between the total f_{esc} computed from Method 2 (§3.2) from UV SED fitting: $f_{\text{esc,tot}}$ and various indirect tracers of f_{esc} : Ly α equivalent width (upper left), [OIII]/[OII] ratio (upper middle), Δ [SII] (upper right), Ly β residual flux (lower left), H β equivalent width (lower middle), and star formation rate surface density (lower right). Symbols are similar to the previous figure. For each figure, the Kendall’s τ coefficient between the x and y values and the probability of the null hypothesis (p) are shown at the corner (red: LzLCS+ & massive leakers, black: only LzLCS+). In all the measured correlations shown above, the significance of the relation (τ) diminishes when the massive leakers are taken into account (marked in red) compared to the correlation observed in the LzLCS+ sample (blue). The observed difference in correlations from Fig. 8 represent is primarily due to dust.

tion modeling (Method 2 in §3.2), replacing F_{900}/F_{1100} . The changes observed on the Y-axis compared to Fig. 8 reflect the significant impact of dust attenuation on the resulting escape fraction that ultimately escapes into the IGM, as highlighted previously.

4.3. Are these a different class of leakers?

We have discussed in the previous section that the massive leakers show some notable differences from the other LyC leaking galaxies in regard to indirect f_{esc} indicators. Particularly, they do not follow the trends of leakiness correlating with primarily in O $_{32}$, or the Ly α and H β EW. Here we evaluate the relationship between a few other host galaxy properties for the massive leakers, and compare them to the LzLCS+ galaxies. Fig. 10 shows the galaxy distributions in three different planes – star formation rate derived from the extinction-corrected UV 1500 Å luminosity (SFR_{UV}) vs. stellar mass (left panel), UV extinction vs. metallicity (middle panel), and H β EW vs Ly α EW (right panel). It is clear

that our sources are more massive, have higher SFR (but lower SFR/M_*), and also very high SFR/Area than the typical LzLCS+ galaxies. These also have significantly higher dust extinction and higher metallicities than the LzLCS+ galaxies, but comparatively weaker emission lines. Thus, these massive leakers differ significantly from the population of ‘traditional’ leakers in the literature. This is further supported by the different emission-line properties of the ISM described in the previous section.

We agree with the hypothesis put forward by Heckman et al. (2011); Borthakur et al. (2014); Alexandroff et al. (2015); Wang et al. (2019); Flury et al. (2022b); Jaskot et al. (2024a) that the LyC escape in these massive leakers is made possible by the extreme feedback effects produced by an extremely massive and compact starburst (Flury et al. 2024). In the three massive leakers discussed by Borthakur et al. (2014) and Wang et al. (2019), the UV light from starburst was dominated by highly compact (marginally resolved by

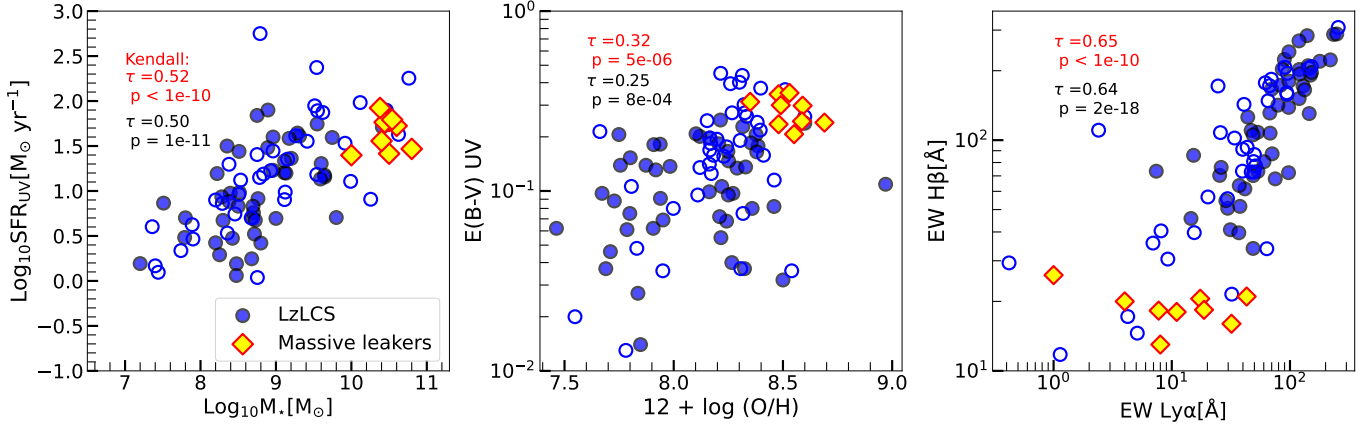


Figure 10. Comparison of galaxy properties between the massive leaker population (yellow diamonds) and the LzLCS+ leakers (blue filled circles), with non-leakers from the LzLCS+ sample represented by hollow symbols. The distributions are shown in three different parameter spaces: star formation rate derived from extinction-corrected UV 1500 Å luminosity (SFR_{UV}) vs. stellar mass (left panel), UV extinction vs. metallicity (middle panel), and $H\beta$ equivalent width vs. $Ly\alpha$ equivalent width (right panel). The massive leakers exhibit higher SFRs (but lower SFR/M_*), greater dust extinction, higher metallicity, and weaker emission lines compared to typical LzLCS+ galaxies, indicating significant differences from traditional leakers in the literature.

HST), massive objects located at or near the galactic nucleus. These were dubbed Dominant Central Objects (DCOs; Overzier et al. 2009). In this study, we have confirmed LyC emission in three out of the five sources. All three have very high SFR/Area, but only J0121 has the morphology of a compact DCO as shown in Fig. 1. The rest have comparatively extended morphology. This suggests that the more general property of very high SFR/Area is responsible for enabling the escape of LyC photons. The typically large values of the RF in the $Ly\beta$ absorption-line in the massive leakers is fully consistent with a “picket fence” geometry for the HI with holes that are fully ionized, enabling LyC escape and also reducing the relative amount of partially-ionized gas traced by [SII]. It is noteworthy that high SFR/A is correlated with high velocities in the starburst-generated galactic winds (e.g., Heckman et al. 2015, 2017; Davis et al. 2023). This suggests that the ionized holes may be created - at least in part - as a result of the extremely high ram pressure associated with the wind fluid. Indeed, Amorín et al. (2024) recently found correlations between the velocity of these feedback driven winds and the LyC escape fraction, while Flury et al. (2024) explored the in-depth connections between the different types of feedback mechanism and the LyC escape. Our low-resolution HST/COS data could not confirm blueshifts in the absorption lines indicative of outflows. We are currently planning follow-up observations with the Large Binocular Telescope to obtain higher spectral resolution data. This analysis will be addressed in future work.

5. CONCLUSIONS

We present HST/COS spectroscopy observations of five low-redshift ($z \sim 0.3$) starburst galaxies, selected for their high stellar mass ($M_\odot > 10^{10}$) and relatively weak [S II]

6717Å, 6731Å nebular emission lines compared to typical star-forming galaxies. The weakness in [S II] is hypothesized to indicate galaxies that are optically thin to ionizing radiation. Recently, several high-redshift galaxies ($z > 5$) observed with JWST have also shown extremely weak [S II] emission (Sanders et al. 2023; Cameron et al. 2023), reinforcing the potential of weak [S II] as a marker of LyC escape in high- z galaxies.

Significant Lyman continuum (LyC) flux was detected in three of the five galaxies, with dust-corrected escape fractions ($f_{esc,corr}$) of 71%, 84%, and 33%, representing the fraction of LyC photons that would escape in the absence of dust. However, the total escape fraction, which is the real fraction of photons escaping into the IGM the effects of both hydrogen absorption and dust extinction, is significantly lower, ranging from 1-3%.

We compared these [S II]-weak galaxies to other known classes of LyC-leaking galaxies. In contrast to the low-redshift traditional leakers from the LzLCS+ sample, these galaxies exhibit higher stellar masses, greater metallicities, more dust extinction, lower ionization states (as indicated by [OIII]/[OII]), smaller $Ly\alpha$ and $H\beta$ equivalent widths, and higher star formation rate surface densities. These results indicate that the massive leakers in our sample constitute a distinct population from the traditional LzLCS+ leakers, suggesting the presence of multiple mechanisms facilitating LyC photon escape. The characteristics of these massive leakers align with a “picket-fence” model, in which intense feedback creates channels or holes in the neutral hydrogen, allowing LyC photons to escape through these openings. This expands the range of galaxy properties over which searches for LyC-leaking galaxies can be conducted, enhancing our ability to use low-redshift leakers as local analogs for studying

the physical processes that allow LyC photons to escape. It also points to the likelihood that various physical conditions and mechanisms contribute to LyC leakage.

- 1 M.J.H. is supported by the Swedish Research Council
- 2 (Vetenskapsradet) and is Fellow of the Knut & Alice Wal-
- 3 lenberg Foundation.

REFERENCES

- Alavi, A., Colbert, J., Teplitz, H. I., et al. 2020, *ApJ*, 904, 59, doi: [10.3847/1538-4357/abbd43](https://doi.org/10.3847/1538-4357/abbd43)
- Alexandroff, R. M., Heckman, T. M., Borthakur, S., Overzier, R., & Leitherer, C. 2015, *ApJ*, 810, 104, doi: [10.1088/0004-637X/810/2/104](https://doi.org/10.1088/0004-637X/810/2/104)
- Amorín, R. O., Rodríguez-Henríquez, M., Fernández, V., et al. 2024, *A&A*, 682, L25, doi: [10.1051/0004-6361/202449175](https://doi.org/10.1051/0004-6361/202449175)
- Atek, H., Labbé, I., Furtak, L. J., et al. 2024, *Nature*, 626, 975, doi: [10.1038/s41586-024-07043-6](https://doi.org/10.1038/s41586-024-07043-6)
- Bañados, E., Carilli, C., Walter, F., et al. 2018, *ApJL*, 861, L14, doi: [10.3847/2041-8213/aac511](https://doi.org/10.3847/2041-8213/aac511)
- Baldwin, J. A., Phillips, M. M., & Terlevich, R. 1981, *PASP*, 93, 5, doi: [10.1086/130766](https://doi.org/10.1086/130766)
- Becker, R. H., Fan, X., White, R. L., et al. 2001, *AJ*, 122, 2850, doi: [10.1086/324231](https://doi.org/10.1086/324231)
- Bergvall, N., Zackrisson, E., Andersson, B. G., et al. 2006, *A&A*, 448, 513, doi: [10.1051/0004-6361:20053788](https://doi.org/10.1051/0004-6361:20053788)
- Borthakur, S., Heckman, T. M., Leitherer, C., & Overzier, R. A. 2014, *Science*, 346, 216, doi: [10.1126/science.1254214](https://doi.org/10.1126/science.1254214)
- Bouwens, R. J., Smit, R., Labbé, I., et al. 2016, *ApJ*, 831, 176, doi: [10.3847/0004-637X/831/2/176](https://doi.org/10.3847/0004-637X/831/2/176)
- Bouwens, R. J., Illingworth, G. D., Oesch, P. A., et al. 2011, *ApJ*, 737, 90, doi: [10.1088/0004-637X/737/2/90](https://doi.org/10.1088/0004-637X/737/2/90)
- Calzetti, D., Armus, L., Bohlin, R. C., et al. 2000, *ApJ*, 533, 682, doi: [10.1086/308692](https://doi.org/10.1086/308692)
- Cameron, A. J., Saxena, A., Bunker, A. J., et al. 2023, arXiv e-prints, arXiv:2302.04298, doi: [10.48550/arXiv.2302.04298](https://doi.org/10.48550/arXiv.2302.04298)
- Chisholm, J., Rigby, J. R., Bayliss, M., et al. 2019, *ApJ*, 882, 182, doi: [10.3847/1538-4357/ab3104](https://doi.org/10.3847/1538-4357/ab3104)
- Chisholm, J., Saldana-Lopez, A., Flury, S., et al. 2022, *MNRAS*, 517, 5104, doi: [10.1093/mnras/stac2874](https://doi.org/10.1093/mnras/stac2874)
- Davis, J. D., Tremonti, C. A., Swiggum, C. N., et al. 2023, *ApJ*, 951, 105, doi: [10.3847/1538-4357/acbbf](https://doi.org/10.3847/1538-4357/acbbf)
- Deharveng, J. M., Buat, V., Le Brun, V., et al. 2001, *A&A*, 375, 805, doi: [10.1051/0004-6361:20010920](https://doi.org/10.1051/0004-6361:20010920)
- Fan, X., Carilli, C. L., & Keating, B. 2006, *ARA&A*, 44, 415, doi: [10.1146/annurev.astro.44.051905.092514](https://doi.org/10.1146/annurev.astro.44.051905.092514)
- Ferland, G. J., Chatzikos, M., Guzmán, F., et al. 2017, *RMxAA*, 53, 385, doi: [10.48550/arXiv.1705.10877](https://doi.org/10.48550/arXiv.1705.10877)
- Finkelstein, S. L., D'Aloisio, A., Paardekoooper, J.-P., et al. 2019, *ApJ*, 879, 36, doi: [10.3847/1538-4357/ab1ea8](https://doi.org/10.3847/1538-4357/ab1ea8)
- Flury, S. R., Jaskot, A. E., Ferguson, H. C., et al. 2022a, *ApJS*, 260, 1, doi: [10.3847/1538-4365/ac5331](https://doi.org/10.3847/1538-4365/ac5331)
- . 2022b, *ApJ*, 930, 126, doi: [10.3847/1538-4357/ac61e4](https://doi.org/10.3847/1538-4357/ac61e4)
- Flury, S. R., Jaskot, A. E., Saldana-Lopez, A., et al. 2024, arXiv e-prints, arXiv:2409.12118, doi: [10.48550/arXiv.2409.12118](https://doi.org/10.48550/arXiv.2409.12118)
- Gazagnes, S., Chisholm, J., Schaerer, D., Verhamme, A., & Izotov, Y. 2020, *A&A*, 639, A85, doi: [10.1051/0004-6361/202038096](https://doi.org/10.1051/0004-6361/202038096)
- Giammanco, C., Beckman, J. E., & Cedrés, B. 2005, *A&A*, 438, 599, doi: [10.1051/0004-6361:20042268](https://doi.org/10.1051/0004-6361:20042268)
- Green, J. C., Froning, C. S., Osterman, S., et al. 2012, *ApJ*, 744, 60, doi: [10.1088/0004-637X/744/1/6010.1086/141956](https://doi.org/10.1088/0004-637X/744/1/6010.1086/141956)
- Heckman, T., Borthakur, S., Wild, V., Schiminovich, D., & Bordoloi, R. 2017, *ApJ*, 846, 151, doi: [10.3847/1538-4357/aa80dc](https://doi.org/10.3847/1538-4357/aa80dc)
- Heckman, T. M., Alexandroff, R. M., Borthakur, S., Overzier, R., & Leitherer, C. 2015, *ApJ*, 809, 147, doi: [10.1088/0004-637X/809/2/147](https://doi.org/10.1088/0004-637X/809/2/147)
- Heckman, T. M., Hoopes, C. G., Seibert, M., et al. 2005, *ApJL*, 619, L35, doi: [10.1086/425979](https://doi.org/10.1086/425979)
- Heckman, T. M., Borthakur, S., Overzier, R., et al. 2011, *ApJ*, 730, 5, doi: [10.1088/0004-637X/730/1/5](https://doi.org/10.1088/0004-637X/730/1/5)
- Hoopes, C. G., Heckman, T. M., Salim, S., et al. 2007, *ApJS*, 173, 441, doi: [10.1086/516644](https://doi.org/10.1086/516644)
- Iwata, I., Inoue, A. K., Matsuda, Y., et al. 2009, *ApJ*, 692, 1287, doi: [10.1088/0004-637X/692/2/1287](https://doi.org/10.1088/0004-637X/692/2/1287)
- Izotov, Y. I., Guseva, N. G., Fricke, K. J., & Henkel, C. 2016a, *MNRAS*, 462, 4427, doi: [10.1093/mnras/stw1973](https://doi.org/10.1093/mnras/stw1973)
- Izotov, Y. I., Guseva, N. G., Fricke, K. J., et al. 2021, *A&A*, 646, A138, doi: [10.1051/0004-6361/202039772](https://doi.org/10.1051/0004-6361/202039772)
- Izotov, Y. I., Schaerer, D., Thuan, T. X., et al. 2016b, *MNRAS*, 461, 3683, doi: [10.1093/mnras/stw1205](https://doi.org/10.1093/mnras/stw1205)
- Izotov, Y. I., Schaerer, D., Worseck, G., et al. 2018a, *MNRAS*, 474, 4514, doi: [10.1093/mnras/stx3115](https://doi.org/10.1093/mnras/stx3115)
- Izotov, Y. I., Worseck, G., Schaerer, D., et al. 2018b, *MNRAS*, 478, 4851, doi: [10.1093/mnras/sty1378](https://doi.org/10.1093/mnras/sty1378)
- Jaskot, A. E., Silveyra, A. C., Plantinga, A., et al. 2024a, *ApJ*, 972, 92, doi: [10.3847/1538-4357/ad58b9](https://doi.org/10.3847/1538-4357/ad58b9)
- . 2024b, *ApJ*, 973, 111, doi: [10.3847/1538-4357/ad5557](https://doi.org/10.3847/1538-4357/ad5557)
- Kennicutt, R. C., & Evans, N. J. 2012, *ARA&A*, 50, 531, doi: [10.1146/annurev-astro-081811-125610](https://doi.org/10.1146/annurev-astro-081811-125610)
- Kewley, L. J., Dopita, M. A., Sutherland, R. S., Heisler, C. A., & Trevena, J. 2001, *ApJ*, 556, 121, doi: [10.1086/321545](https://doi.org/10.1086/321545)
- Kroupa, P. 2001, *MNRAS*, 322, 231, doi: [10.1046/j.1365-8711.2001.04022.x](https://doi.org/10.1046/j.1365-8711.2001.04022.x)

- Leitherer, C., Ekström, S., Meynet, G., et al. 2014, *ApJS*, 212, 14, doi: [10.1088/0067-0049/212/1/14](https://doi.org/10.1088/0067-0049/212/1/14)
- Leitherer, C., Ferguson, H. C., Heckman, T. M., & Lowenthal, J. D. 1995, *ApJL*, 454, L19, doi: [10.1086/309760](https://doi.org/10.1086/309760)
- Leitherer, C., Hernandez, S., Lee, J. C., & Oey, M. S. 2016, *ApJ*, 823, 64, doi: [10.3847/0004-637X/823/1/64](https://doi.org/10.3847/0004-637X/823/1/64)
- Leitherer, C., Ortiz Otálvaro, P. A., Bresolin, F., et al. 2010, *ApJS*, 189, 309, doi: [10.1088/0067-0049/189/2/309](https://doi.org/10.1088/0067-0049/189/2/309)
- Leitherer, C., Tremonti, C. A., Heckman, T. M., & Calzetti, D. 2011, *AJ*, 141, 37, doi: [10.1088/0004-6256/141/2/37](https://doi.org/10.1088/0004-6256/141/2/37)
- Makan, K., Worseck, G., Davies, F. B., et al. 2021, *ApJ*, 912, 38, doi: [10.3847/1538-4357/abee17](https://doi.org/10.3847/1538-4357/abee17)
- Malkan, M., Webb, W., & Konopacky, Q. 2003, *ApJ*, 598, 878, doi: [10.1086/379117](https://doi.org/10.1086/379117)
- Martin, D. C., Fanson, J., Schiminovich, D., et al. 2005, *ApJL*, 619, L1, doi: [10.1086/426387](https://doi.org/10.1086/426387)
- Mason, C., & GLASS, B. 2018, in *American Astronomical Society Meeting Abstracts*, Vol. 231, American Astronomical Society Meeting Abstracts #231, 226.02
- Meynet, G., Maeder, A., Schaller, G., Schaerer, D., & Charbonnel, C. 1994, *A&AS*, 103, 97
- Overzier, R. A., Heckman, T. M., Schiminovich, D., et al. 2010, *ApJ*, 710, 979, doi: [10.1088/0004-637X/710/2/979](https://doi.org/10.1088/0004-637X/710/2/979)
- Overzier, R. A., Heckman, T. M., Kauffmann, G., et al. 2008, *ApJ*, 677, 37, doi: [10.1086/529134](https://doi.org/10.1086/529134)
- Overzier, R. A., Heckman, T. M., Tremonti, C., et al. 2009, *ApJ*, 706, 203, doi: [10.1088/0004-637X/706/1/203](https://doi.org/10.1088/0004-637X/706/1/203)
- Pauldrach, A. W. A., Hoffmann, T. L., & Lennon, M. 2001, *A&A*, 375, 161, doi: [10.1051/0004-6361:20010805](https://doi.org/10.1051/0004-6361:20010805)
- Pellegrini, E. W., Oey, M. S., Winkler, P. F., et al. 2012, *ApJ*, 755, 40, doi: [10.1088/0004-637X/755/1/40](https://doi.org/10.1088/0004-637X/755/1/40)
- Pettini, M., & Pagel, B. E. J. 2004, *MNRAS*, 348, L59, doi: [10.1111/j.1365-2966.2004.07591.x](https://doi.org/10.1111/j.1365-2966.2004.07591.x)
- Planck Collaboration, Aghanim, N., Akrami, Y., et al. 2020, *A&A*, 641, A1, doi: [10.1051/0004-6361/201833880](https://doi.org/10.1051/0004-6361/201833880)
- Ramambason, L., Schaerer, D., Stasińska, G., et al. 2020, *A&A*, 644, A21, doi: [10.1051/0004-6361/202038634](https://doi.org/10.1051/0004-6361/202038634)
- Reddy, N. A., Steidel, C. C., Pettini, M., Bogosavljević, M., & Shapley, A. E. 2016, *ApJ*, 828, 108, doi: [10.3847/0004-637X/828/2/108](https://doi.org/10.3847/0004-637X/828/2/108)
- Robertson, B. E. 2022, *ARA&A*, 60, 121, doi: [10.1146/annurev-astro-120221-044656](https://doi.org/10.1146/annurev-astro-120221-044656)
- Robertson, B. E., Ellis, R. S., Furlanetto, S. R., & Dunlop, J. S. 2015, *ApJL*, 802, L19, doi: [10.1088/2041-8205/802/2/L19](https://doi.org/10.1088/2041-8205/802/2/L19)
- Roy, N., Henry, A., Treu, T., et al. 2023, *ApJL*, 952, L14, doi: [10.3847/2041-8213/acdbce](https://doi.org/10.3847/2041-8213/acdbce)
- Saldana-Lopez, A., Schaerer, D., Chisholm, J., et al. 2022, *A&A*, 663, A59, doi: [10.1051/0004-6361/202141864](https://doi.org/10.1051/0004-6361/202141864)
- Sanders, R. L., Shapley, A. E., Topping, M. W., Reddy, N. A., & Brammer, G. B. 2023, *arXiv e-prints*, arXiv:2301.06696, doi: [10.48550/arXiv.2301.06696](https://doi.org/10.48550/arXiv.2301.06696)
- Sawant, A. N., Pellegrini, E. W., Oey, M. S., López-Hernández, J., & Micheva, G. 2021, *ApJ*, 923, 78, doi: [10.3847/1538-4357/ac2c85](https://doi.org/10.3847/1538-4357/ac2c85)
- Stasińska, G., Izotov, Y., Morisset, C., & Guseva, N. 2015, *A&A*, 576, A83, doi: [10.1051/0004-6361/201425389](https://doi.org/10.1051/0004-6361/201425389)
- Steidel, C. C., Bogosavljević, M., Shapley, A. E., et al. 2018, *ApJ*, 869, 123, doi: [10.3847/1538-4357/aaed28](https://doi.org/10.3847/1538-4357/aaed28)
- Thomas, D., Steele, O., Maraston, C., et al. 2013, *MNRAS*, 431, 1383, doi: [10.1093/mnras/stt261](https://doi.org/10.1093/mnras/stt261)
- Veilleux, S., & Osterbrock, D. E. 1987, *ApJS*, 63, 295, doi: [10.1086/191166](https://doi.org/10.1086/191166)
- Wang, B., Heckman, T. M., Leitherer, C., et al. 2019, *ApJ*, 885, 57, doi: [10.3847/1538-4357/ab418f](https://doi.org/10.3847/1538-4357/ab418f)
- Wang, B., Heckman, T. M., Amorín, R., et al. 2021, *ApJ*, 916, 3, doi: [10.3847/1538-4357/ac0434](https://doi.org/10.3847/1538-4357/ac0434)
- Worseck, G., Prochaska, J. X., Hennawi, J. F., & McQuinn, M. 2016, *ApJ*, 825, 144, doi: [10.3847/0004-637X/825/2/144](https://doi.org/10.3847/0004-637X/825/2/144)
- Xu, X., Henry, A., Heckman, T., et al. 2022, *ApJ*, 933, 202, doi: [10.3847/1538-4357/ac7225](https://doi.org/10.3847/1538-4357/ac7225)
- . 2023, *ApJ*, 943, 94, doi: [10.3847/1538-4357/aca89a](https://doi.org/10.3847/1538-4357/aca89a)
- York, D. G., Adelman, J., Anderson, John E., J., et al. 2000, *AJ*, 120, 1579, doi: [10.1086/301513](https://doi.org/10.1086/301513)